Available online at www.sciencedirect.com
SCIENCE DIRECT®
International Journal of Heat and Fluid Flow 25 (2004) 115–126
International Journal of HEAT AND FLUID FLOW
www.elsevier.com/locate/ijhff

Mathematical model and simulation of gas flow through a porous medium in high breaking capacity fuses

D. Rochette [a], S. Clain [b,*]

[a] Laboratoire Arc Electrique et Plasmas thermiques, Université Blaise Pascal, CNRS UMR 6069, Phys. Bât. 5, 24 Avenue des Landais, F 63177 Aubière Cedex, France
[b] Laboratoire Mathématiques Appliquées, Université Blaise Pascal, CNRS UMR 6620, 24 Avenue des Landais, F 63177 Aubière Cedex, France

Received 3 February 2003; accepted 11 September 2003

Abstract

We present a one-dimensional model to describe the gas flow and the heat transfer in high breaking capacity (HBC) fuses. The compressible Euler equations for perfect gas have been used as the basic flow model coupled with a porous medium model taking into account the mechanical interaction between the gas and the silica sand and the heat transfer between hot gas and cold silica sand. In addition, to describe the solid temperature evolution, we introduce the heat equation for the solid. The governing equations are discretized following a finite volume scheme coupled with a fractional step technique and the fluxes are evaluated using the Roe method. The computational fluid dynamics model is used for the numerical investigations of a gas-flow in a porous medium for HBC fuses.

Keywords: Porous media; Heat transfer; Thermal non-equilibrium; Darcy; Forchheimer; Finite-volume; Fuse

1. Introduction

High breaking capacity (HBC) fuses are widely used to ensure a specific current limit. They are composed of a silver conducting element surrounded by a porous medium: the silica sand. During the arcing, an experimental HBC fuse is compounded of two principle regions as shown schematically in Fig. 1. A plasma area is roughly a parallelepiped taking place in the silica sand with the same $(0y)$ and $(0z)$ dimensions of the fuse and a thin depth following $(0x)$.

Due to the symmetry, the phenomenon is invariant following $(0y)$ and $(0z)$ axes, so we only consider the x-positive domain and we state that physical parameters only depend on the space variable x and time variable t (see Fig. 2). The first region is the arc core located in the interval $[0, \delta]$ representing the plasma zone contained in the silica sand, lying in the domain $[0, L]$.

The physical mechanisms responsible for the arc plasma evolution during the fuse operation have been widely studied (Lakshiminarashima et al., 1978; Turner and Turner, 1973; Bussière and Bezborodko, 1999):

- overheating of the silver fuse element leading to the fusion and the vaporization of the metal;
- creation of an electrical arc;
- fusion and vaporization of the silica sand;
- energy dissipation from the arc column to the porous medium which is used as an arc-quenching medium.

The process in the circuit-breakers involves a compressible gas flow from low to high speed through a porous medium, the presence of important exchanges of energy by heat transfer between hot gas and cold silica, the creation and the condensation of gaseous material.

To describe the evolution of physical parameters such that the gas velocity, the pressure and the temperature we use the Euler equations taking into account the presence of a porous medium since the morphology of silica grains influences the arc behaviour in HBC fuses (Bussière, 2001).

* Corresponding author. Tel.: +33-473-407055; fax: +33-473-407064.
E-mail address: stephane.clain@math.univ-bpclermont.fr (S. Clain).

0142-727X/$ - see front matter © 2003 Elsevier Inc. All rights reserved.
doi:10.1016/j.ijheatfluidflow.2003.09.001

Nomenclature

A_0	specific surface area (m^{-1})
c_p, c_v	specific heat ($J\,kg^{-1}\,K^{-1}$)
D	mass flow rate ($kg\,m^{-2}\,s^{-1}$)
d	particle diameter (m)
e	specific internal energy ($J\,kg^{-1}$)
E	total energy ($J\,m^{-3}$)
h_{sf}	heat transfer coefficient
k	permeability (m^2)
k_g	gas thermal conductivity ($W\,m^{-1}\,K^{-1}$)
k_{eff}	effective thermal conductivity ($W\,m^{-1}\,K^{-1}$)
Nu	Nusselt number
p	pressure (Pa)
Pr	Prandtl number
r	mass source ($kg\,m^{-3}\,s^{-1}$)
Re	Reynolds number
S	energy source
T_g, T_s	gas and solid temperature (K)
u	interstitial velocity ($m\,s^{-1}$)
U	vector of independent variables

Greeks

β	Forchheimer coefficient (m^{-1})
γ	adiabatique index
ϕ	porosity
μ	gas viscosity ($kg\,m^{-1}\,s^{-1}$)
ρ_g, ρ_s	gas and solid density ($kg\,m^{-3}$)

Subscripts

g	gas
in	channel inlet
out	channel outlet
s	solid
sf	interfacial conditions

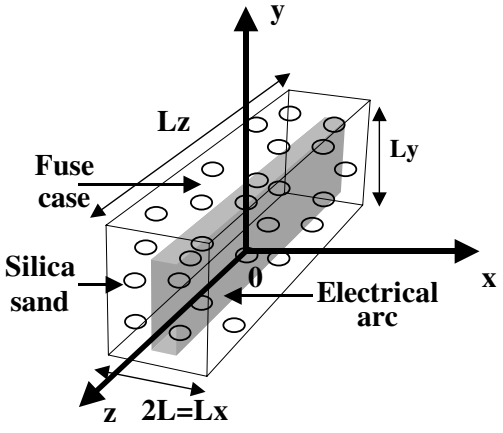

Fig. 1. Geometry of the studied experimental fuse.

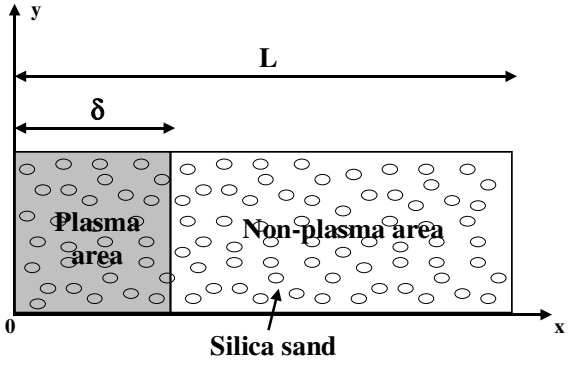

Fig. 2. One-dimensional geometry of the fuse process.

Usually, the gas–silica sand interaction is governed by a relationship between the pressure drop and the flow rate through porous medium, it depends on the nature and the velocity of the fluid as well as the silica grain morphology. It is well known that, in first approximation, the pressure drop is linearly proportional to the flow rate (Darcy's law). At high flow rates, the pressure drop exceeds the one predicted by Darcy's law and this phenomenon is known as the Forchheimer flow behaviour. It is primarily due to the inertial term in Euler equations and the turbulence. To take into account the Forchheimer behaviour of the flow, authors suggest some additional laws (Whitaker, 1996; Rohsenow et al., 1998).

A large part of the energy contained in the hot gas is transmitted into the cold silica sand. To describe the interfacial heat transfer, several authors (Rohsenow et al., 1998; Jiang and Ren, 2001) propose empiric laws linking the energy transfer with the gas temperature and the dimensionless numbers such that the Reynolds, Nusselt, Prandtl numbers.

The plasma induces a local vaporization of the material (the silver fuse element and the silica sand surrounding the arc plasma) which highly influences the total gas density, thus the pressure. A vaporization rate is then introduced in the mass conservation equation mainly due to the silica sand vaporization since the silver vapour contribution is negligible in the plasma (Bussière, 2000).

From the technological point of view, the pressure role is fundamental during a short-circuit current interruption because a high plasma pressure induces a fuse voltage which is larger than the system voltage and thus the fuse dissipates more quickly all the energy contained in the system and favours the arc plasma extinction. The high plasma pressure depends

on the arc temperature and the rate of vaporized material. Several authors have shown that the pressure behaviour is also conditioned by the surrounding silica sand (Bussière, 2001) since it confines the electrical arc and contributes to vaporize material. On the other hand, the silver vapours contained in the plasma due to the silver fuse element vaporization must be ejected through the silica sand to avoid a reignition of the plasma.

To model the short-circuit current interruption process, we assume that the plasma is in local thermodynamic equilibrium (Bussière and André, 2001), allowing to use the same Euler equations for all gaseous species, but to evaluate the porous media temperature evolution, we use a thermal non-equilibrium model between the gas and the porous media. Furthermore, we include a mass source term to represent the mass produced by vaporization, an impulsion source term to represent interaction gas–silica in introducing Darcy's law and Forchheimer's law (De Ville, 1996; Macdonald et al., 1979; Teng and Zhao, 2000; Whitaker, 1996) and an energy source term to represent electrical energy and heat transfer between gas and silica sand grains describes by an empiric law depending on the process (Rohsenow et al., 1998; Jiang and Ren, 2001).

The aim of this paper is to compute the evolution of the pressure, the gas velocity and the temperature during the fuse operation using realistic values for the silica sand (permeability, Forchheimer coefficient). Moreover, we want to locate the areas where the Darcy and Forchheimer forces are dominant as well as the repartition of the heat transfer.

The paper is organized in the following way: in Section 2, the mathematical model presents Euler equations and source terms. Section 3 is devoted to numerical method to obtain an approximated solution, we use a finite volume scheme based on a Roe's solver and a fractional step technique. In the last section, some numerical results obtained for a one-dimensional geometry are presented.

2. Mathematical model

In this model, we are interested in the evolution of physical values of the gas and we do not take into account the liquid phase motion. The one-dimensional governing equations for single-phase fluid flow in an isotropic, homogeneous porous medium based on the Brinkman–Darcy–Forchheimer model (Jiang and Ren, 2001) can be written in the following form:

Mass conservation

$$\frac{\partial(\rho_g\phi)}{\partial t}+\frac{\partial(\rho_g\phi u)}{\partial x}=r. \tag{1}$$

Momentum conservation

$$\frac{\partial(\rho_g\phi u)}{\partial t}+\frac{\partial(\rho_g\phi u^2+\phi p)}{\partial x}=p\frac{\partial\phi}{\partial x}-\phi^2\frac{\mu}{k}u-\phi^3\beta\rho_g|u|u+\frac{\partial}{\partial x}\left(\phi\mu\frac{\partial u}{\partial x}\right). \tag{2}$$

Energy conservation

$$\frac{\partial(\phi E)}{\partial t}+\frac{\partial[(E+p).\phi u]}{\partial x}=pu\frac{\partial\phi}{\partial x}+S-h_{sf}A_0(T_g-T_s). \tag{3}$$

The physical parameters are ρ_g the density, u the interstitial velocity, p the pressure, ϕ the porosity and E the total energy per unit volume defined by

$$E=\rho_g(\tfrac{1}{2}u^2+e)\quad\text{with } e=c_{vg}T_g, \tag{4}$$

where e is the specific internal energy and T_g the gas temperature.

In Eq. (1), the quantity r represents the material source due to the vaporization of material.

In Eq. (2), the expression $-\phi^2\frac{\mu}{k}u$ represents the viscous friction between gas and grains of silica sand where μ is the dynamic viscosity, k is the medium permeability and the term $-\phi^3\beta\rho|u|u$ is the Forchheimer flow resistance where β is the Forchheimer coefficient. In our model, the Brinkman correction is neglected and the electromagnetic force is omitted since the electromagnetic field is confined in the plasma by the surrounding sand and in the plasma, the Laplace force is negligible in comparison with the pressure gradient. Moreover, the sand is assumed incompressible, therefore $\frac{\partial\phi}{\partial x}$ vanishes.

In Eq. (3), S represents the electrical energy injected in the fuse per unit volume and the quantity $h_{sf}A_0(T_g-T_s)$ is the thermal dispersion representing heat exchanges between gas and silica sand.

In addition, to close the system we use the ideal gas equation of state

$$p(\rho_g,e)=(\gamma-1)\rho_g e\quad\text{with } \gamma>1, \tag{5}$$

where γ is the ratio of specific heat capacities of the gas. The ideal gas assumption is valid in the range $T<30\,000$ K since the Debye–Huckel correction (André et al., 2002) does not noticeably affect the high pressure in the plasma core.

The system of equations can be expressed in the general conservative form:

$$\frac{\partial U}{\partial t}+\frac{\partial F(U)}{\partial x}=S(U) \tag{6}$$

with

$$U=\begin{pmatrix}\rho_g\phi\\ \rho_g\phi u\\ \phi E\end{pmatrix},\quad F(U)=\begin{pmatrix}\rho_g\phi u\\ \rho_g\phi u^2+\phi p\\ (E+p).\phi u\end{pmatrix}, \tag{7}$$

where U is a vector of conservative variables and $F(U)$, $S(U)$ are respectively the flux vector and the source

vector regarded as functions of the conserved variable vector U and the fixed parameters. To set boundary conditions, we use the symmetry condition at $x = 0$ which yields $\frac{\partial \rho}{\partial x}(0,t) = 0$, $u(0,t) = 0$ and $\frac{\partial E}{\partial x}(0,t) = 0$. At $x = L$ we assume that the gas is at atmospheric conditions presented in Section 4.3.

To model the heat transfer processes with a thermal non-equilibrium between the gas and solid phases, we introduce the classical heat equation with longitudinal thermal conduction in the solid phase (Bortolozzi and Deiber, 2001) to evaluate the solid temperature T_s:

$$\rho_s c_{vs} \frac{\partial T_s}{\partial t} = \frac{k_{eff}}{(1-\phi)} \frac{\partial^2 T_s}{\partial x^2} + \frac{h_{sf} A_0}{(1-\phi)} (T_g - T_s), \tag{8}$$

where ρ_s denotes the solid density, c_{vs} is the solid specific heat at constant volume and k_{eff} is the porous media conductivity.

3. Source terms

3.1. Mass source term

An excess current generates heat at the constrictions of silver element fuse and leads to fusion and vaporization of the silver at the beginning and vaporization of the silica sand later. The silver fuse element thickness is negligible in comparison with the silica sand grains, so in a first approximation, we assume that the rate of vaporized mass is proportional to the electrical power injected in the fuse and the mass source term computation involves the enthalpy of vaporization of the silica sand (Claessens et al., 1997) fitted by a percentage of the electrical power (Nielsen et al., 2001). The mass source term is given by

- if x is in the plasma cells (i.e. $x \leqslant \delta$) then
  - if $T < T_{vap}(SiO_2)$, $r(x,t) = 0$,
  - if $T \geqslant T_{vap}(SiO_2)$, $r(x,t) = \delta_{SiO_2} \frac{S(x,t)}{H_{vap}(SiO_2)}$,
- if x is not in the plasma cells (i.e. $x > \delta$) then $r(x,t) = 0$,

where $\delta_{SiO_2} \in [0,1]$, represents the percentage of electrical power responsible of silica sand vaporization. The enthalpy of vaporization of silica sand is noted by $H_{vap}(SiO_2)$. The function $S(x,t)$ is the electrical power density presented in the following section.

3.2. Energy source term

In this model, we do not take into account the radiation effect. The electrical arc is confined by the silica sand and we assume that the total power radiated by the arc is immediately absorbed inducing a local silica vaporization in the plasma arc zone. From a macroscopic point of view, the homogeneization makes the radiation energy negligible in the energy equation but the vaporization is taken into account in the source terms.

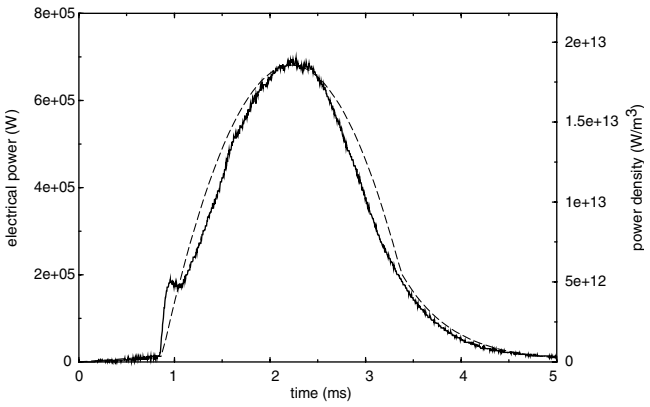

Fig. 3. The solid line and the dash line represent respectively the total electric power $P_{exp}(t)$ and the power density $S(x,t)$ injected in the experimental fuse.

The energy source term has contributions from electrical power and thermal dissipation. From experimental fuses (Bussière and Bezborodko, 1999), we obtain electrical characteristics: voltage $U(t)$, electric current $I(t)$ and total electrical power $P_{exp}(t) = U(t)I(t)$ (see Fig. 3).

This electrical energy injected is characterized by a power density function, denoted by $S(x,t)$, representing the energy quantity injected per unit volume and time (see Fig. 3). The power is mainly injected in the plasma area where we assume an uniform distribution given by:

- if x is in the plasma cells then $S(x,t) = \frac{P_{exp}(t)}{vol}$,
- if x is not in the plasma cells then $S(x,t) = 0$,

where $vol = \delta \cdot L_y \cdot L_z$ is the plasma volume (see Fig. 1).

An important part of the energy injected in the fuse is dissipated by transfer between the hot gas and the cold silica sand. Following Rohsenow et al. (1998), Jiang and Ren (2001) and Jakubiuk and Lipski (1993), the modelling of the heat transfer between gas and silica sand is given by

$$Q = h_{sf} A_0 (T_g - T_s), \tag{9}$$

where T_g is the gas temperature computed by Eq. (4), T_s is the silica sand temperature computed by Eq. (8) and $A_0 = A_{sf}/V_s$ is the specific surface area. The $h_{sf}(x,t)$ function represents the interfacial convection heat transfer coefficient; it depends on the gas nature, the gas flow regime (described by Reynolds number) and the morphology and roughly of silica sand grains.

The h_{sf} function is estimated by empiric laws (Rohsenow et al., 1998), it has been shown that it depends on three dimensionless numbers: the Reynolds number $Re = (\rho_g u \phi d)/\mu$, the Prandtl number $Pr = (\mu c_{pg})/k_g$ and

the Nusselt number $Nu = (h_{sf}d)/k_g$. Wakao and Kaguei (1982) have found the following correlation for h_{sf} given by $Nu \approx 2 + 1.1Re^{0.6}Pr^{1/3}$. Here, we take $A_0 = [6(1-\phi)]/d$ as Jiang and Ren (2001) and the expression for heat exchange writes

$$Q = \frac{k_g Nu(x,t)}{d}\frac{6(1-\phi)}{d}(T_g - T_s). \tag{10}$$

4. The numerical method

4.1. The fractional step technique

In order to obtain an approximate solution of Eq. (6), we use a fractional step technique (Toro, 1997; Rochette and Clain, 2003): we solve separately during a small time step Δt on the one hand the homogeneous conservative system and on the other hand the right-hand side terms. Let U^n be an approximation of $U(t^n)$ at time t^n. In order to obtain an approximation of $U(t^{n+1})$ at time $t^{n+1} = t^n + \Delta t$, we first determine an approximate solution on the time interval $[t^n, t^{n+1}]$ of the homogeneous problem using the finite volume scheme presented in Section 4.1.1. Assumed now that $\widetilde{U}^{n+1}$ is the approximated solution value at $t = t^{n+1}$ of the homogeneous problem: $\frac{\partial U}{\partial t} + \frac{\partial F(U)}{\partial x} = 0$, we solve the ordinary differential equation $\frac{dU}{dt} = S(U)$, using $\widetilde{U}^{n+1}$ as initial condition. The value of the solution at $t = t^{n+1}$ is an approximation U^{n+1} of $U(t^{n+1})$.

4.1.1. The homogeneous problem

Briefly, we describe the finite volume method based on a Roe's solver (Toro, 1997). Let us consider an uniform grid of the domain $[0, L]$ setting $x_i = \left(i - \frac{1}{2}\right)\Delta x$ with $i = 1, \ldots, N$ and we let $x_{i-1/2} = x_i - \frac{\Delta x}{2}$. For each index i, $C_i = [x_{i-1/2}, x_{i+1/2}]$ represents the cell of centre x_i and length Δx.

Knowing an approximation U_i^n of $U(x_i, t^n)$ for the time value t^n, constant on the cell C_i, we seek for an approximate $\widetilde{U}^{n+1}$ for the homogeneous problem. To compute the approximate solution of the homogeneous problem, we use a finite volume scheme of the form

$$\widetilde{U}_i^{n+1} = U_i^n - \frac{\Delta t}{\Delta x}(F_{i+1/2}^n - F_{i-1/2}^n), \tag{11}$$

where $F_{i+1/2}^n$ and $F_{i-1/2}^n$ represent respectively the numerical flux calculated at the interface cells $x = x_{i+1/2}$ and $x = x_{i-1/2}$ using Roe's solver (Toro, 1997).

The second-order spatial accuracy is obtained thanks to the MUSCL method with slope limited (Yee, 1987; Abgrall, 1988). Moreover, the time step Δt_h is chosen in agreement with the Courant–Friedrichs–Lewy (CFL) condition (Courant and Friedrichs, 1948).

4.1.2. The non-homogeneous problem

The second step consists in solving the first-order systems of ordinary differential equations (Toro, 1997; Rochette and Clain, 2003):

$$\frac{dU}{dt} = S(U) = \begin{pmatrix} \frac{r(x,t)}{\phi} \\ -\phi\frac{\mu}{k}u - \phi^2\beta\rho|u|u \\ \frac{S(x,t)}{\phi} - \frac{h_{sf}A_0}{\phi}(T_g - T_s) \end{pmatrix}. \tag{12}$$

Numerically, we add the right-hand side contribution using a fourth-order explicit Runge–Kutta method. Since the method is explicit, a stability condition arises and the time step Δt must be lower to a limit time interval Δt_l.

4.2. Solid energy equation

To compute the solid temperature, we consider the same uniform grid of the domain $[0, L]$. Assume that we know an approximation T_i^n of $T(x_i, t^n)$ at t^n on the cell C_i, we seek for an approximate T_i^{n+1} of the solid heat equation using an explicit finite volume method given by

$$\begin{aligned}\rho_s c_{vs} T_{s,i}^{n+1} = \rho_s c_{vs} T_{s,i}^{n+1} + \frac{\Delta t}{\Delta x}(f_{i+1/2}^n - f_{i-1/2}^n) \\ - \Delta t h_{sf,i}^n A_0 (T_{s,i}^n - T_{f,i}^n),\end{aligned} \tag{13}$$

where central differences are used to determine the fluxes, i.e:

$$f_{i+1/2}^n = k_{eff}\frac{T_{i+1}^n - T_i^n}{\Delta x} \quad \text{and} \quad f_{i-1/2}^n = k_{eff}\frac{T_i^n - T_{i-1}^n}{\Delta x}.$$

It is well known that the explicit scheme is stable if we satisfy the condition $\Delta t_s < [\rho_s c_{vs}(\Delta x)^2]/k_{eff}$. In the application, the CFL condition for the gas flow problem gives a more restrictive condition that the stability condition. Therefore an implicit scheme is not necessary.

4.3. The numerical treatment of the boundary conditions

The fuse operation takes place in a finite domain $[0, L]$ discretized with N cells and closed by edges. Boundary conditions are necessary to complete the flux contribution on the interfaces $x = 0$ and $x = L$. To this end, we use a mirror technique adding a fictitious cell C_0 (symmetry) and transmissive boundary at C_{N+1} (Toro, 1997). For the C_0 cell, we set the mirror condition

$$U_0^n = \begin{pmatrix} \rho_0^n \\ u_0^n \\ P_0^n \end{pmatrix} = \begin{pmatrix} \rho_1^n \\ -u_1^n \\ P_1^n \end{pmatrix}, \tag{14}$$

and for the C_{N+1} cell, we set the transmissive condition

$$U_{N+1}^n = \begin{pmatrix} \rho_{N+1}^n \\ u_{N+1}^n \\ P_{N+1}^n \end{pmatrix} = \begin{pmatrix} 1.2 \\ u_N^n \\ 10^5 \end{pmatrix}. \tag{15}$$

The artificial conditions $\rho_0^n = \rho_1^n$ and $p_0^n = p_1^n$ yield respectively that $\frac{\partial \rho_g}{\partial x}(0, t^n) = 0$ and $\frac{\partial p}{\partial x}(0, t^n) = 0$ which are consistent with the boundary condition of the continuous problem. The condition $u_0^n = -u_1^n$ yields that the velocity vanishes at the boundary. The boundary condition at $x = L$ represents a gas at atmospheric conditions ejected with the velocity u_N^n.

Table 1
Data used in the numerical simulations

Porosity	$\phi = 0.4$
Permeability	$k = 1.5 \times 10^{-11}$ m^2
Forchheimer coefficient	$\beta = 1.35 \times 10^5$ m^{-1}
Particle diameter	$d = 3 \times 10^{-4}$ m
Viscosity	$\mu = 1.8 \times 10^{-5}$ kg m^{-1} s^{-1}
Thermal conductivity of gas	$k_g = 0.026$ W m^{-1} K^{-1}
Effective thermal conductivity of the porous medium	$k_{eff} = 0.33$ W m^{-1} K^{-1}
Gas heat capacity at constant volume	$c_{vg} = 719.3$ J kg^{-1} K^{-1}
Gas heat capacity at constant pressure	$c_{pg} = 1007.0$ J kg^{-1} K^{-1}
Porous medium heat capacity	$c_{ps} = 1420.0$ J kg^{-1} K^{-1}
Adiabatic index	$\gamma = 1.4$
Silica sand enthalpy vaporization	$H_{vap}(SiO_2) = 1.01 \times 10^7$ J kg^{-1}

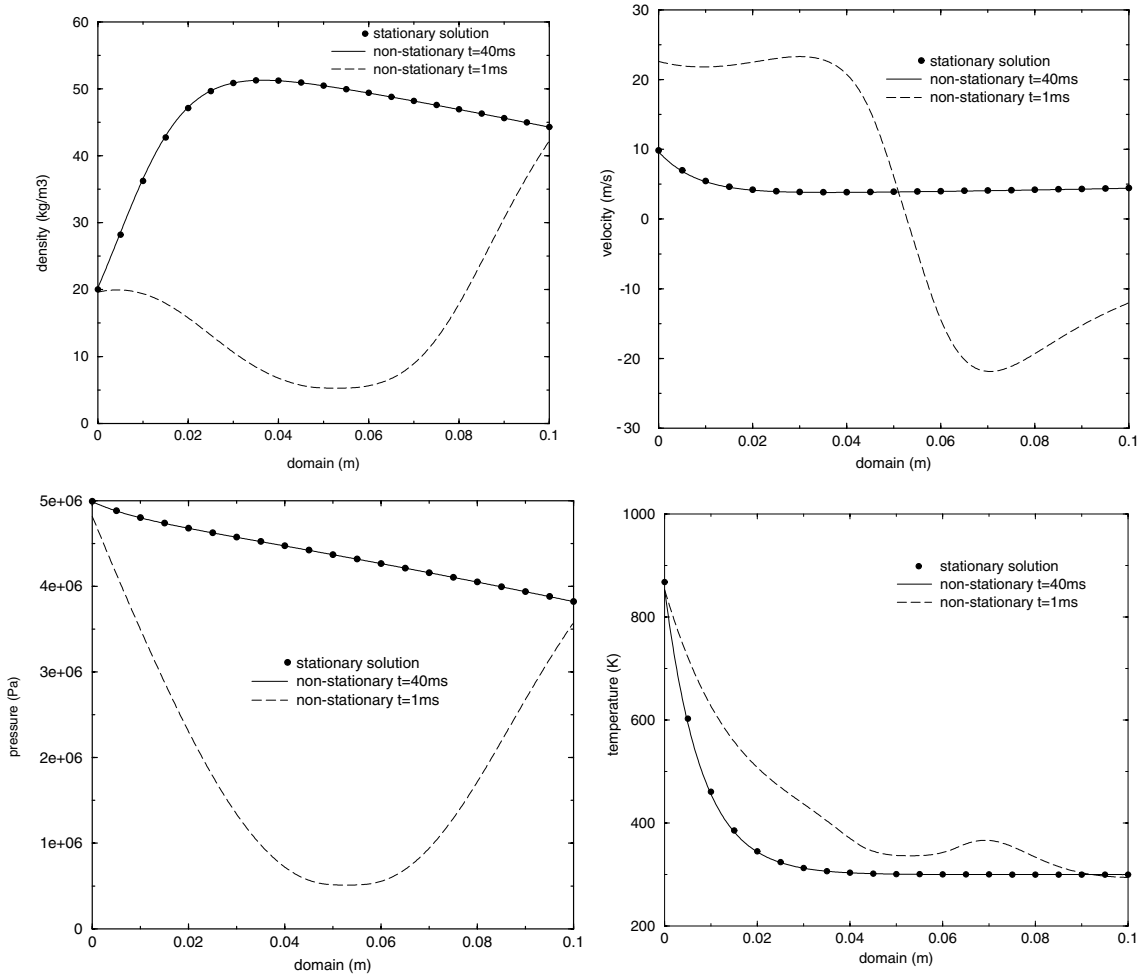

Fig. 4. Comparison of density, velocity, pressure and temperature profiles between the analytic stationary solution (●), numerical solution at time $t = 40$ ms (solid line) and numerical solution at time $t = 1$ ms (dashes line).

5. The stationary solution

An analytic solution of the non-stationary problem is not obvious to obtain, but in the stationary case, it is possible to give a semi-analytic expression of the solution using judicious boundary conditions. To simplify the stationary solution, we assume that the solid temperature T_s and the heat transfer coefficient $h_{sf}A_0$ are constant. We assume that any theoretical non-stationary solution with the same boundary conditions converges asymptotically to the stationary solution. Thus any numerical solution must converge in time to the stationary solution independently of the initial conditions if we impose the same boundary conditions.

Since we want a stationary solution, we have $\frac{\partial \rho}{\partial t} = \frac{\partial u}{\partial t} = \frac{\partial E}{\partial t} = 0$ and Eqs. (1)–(3) yield:

$$
\begin{aligned}
&D = \rho u = \text{constant},\\
&\frac{\mathrm{d}P}{\mathrm{d}x} = 2\gamma D^2\left[\frac{h_{sf}A_0}{\gamma D}\left(T_s\rho(\gamma-1)-\frac{p}{c_v}\right)+\phi p\left(\frac{\mu}{Dk}+\phi\beta\right)\right.\\
&\qquad\left.-\frac{(\gamma-1)}{2\gamma}\phi\left(\frac{\mu}{k}+D\phi\beta\right)\right]\\
&\qquad\times\left[2\gamma D^2-2\gamma\rho P+(\gamma-1)\rho D\right]^{-1},\\
&\frac{\mathrm{d}\rho}{\mathrm{d}x} = \frac{\rho^2}{D^2}\frac{\mathrm{d}P}{\mathrm{d}x}+\frac{\rho}{D}\phi\frac{\mu}{k}+\phi^2\rho\beta,
\end{aligned}
\tag{16}
$$

where D represents the mass flow rate. To solve the stationary problem, we impose inlet boundary conditions and we use a simple forward Euler method. In our example, we have chosen $\rho_{in} = 20.0\ \mathrm{kg\,m^{-3}}$, $u_{in} = 10.0$

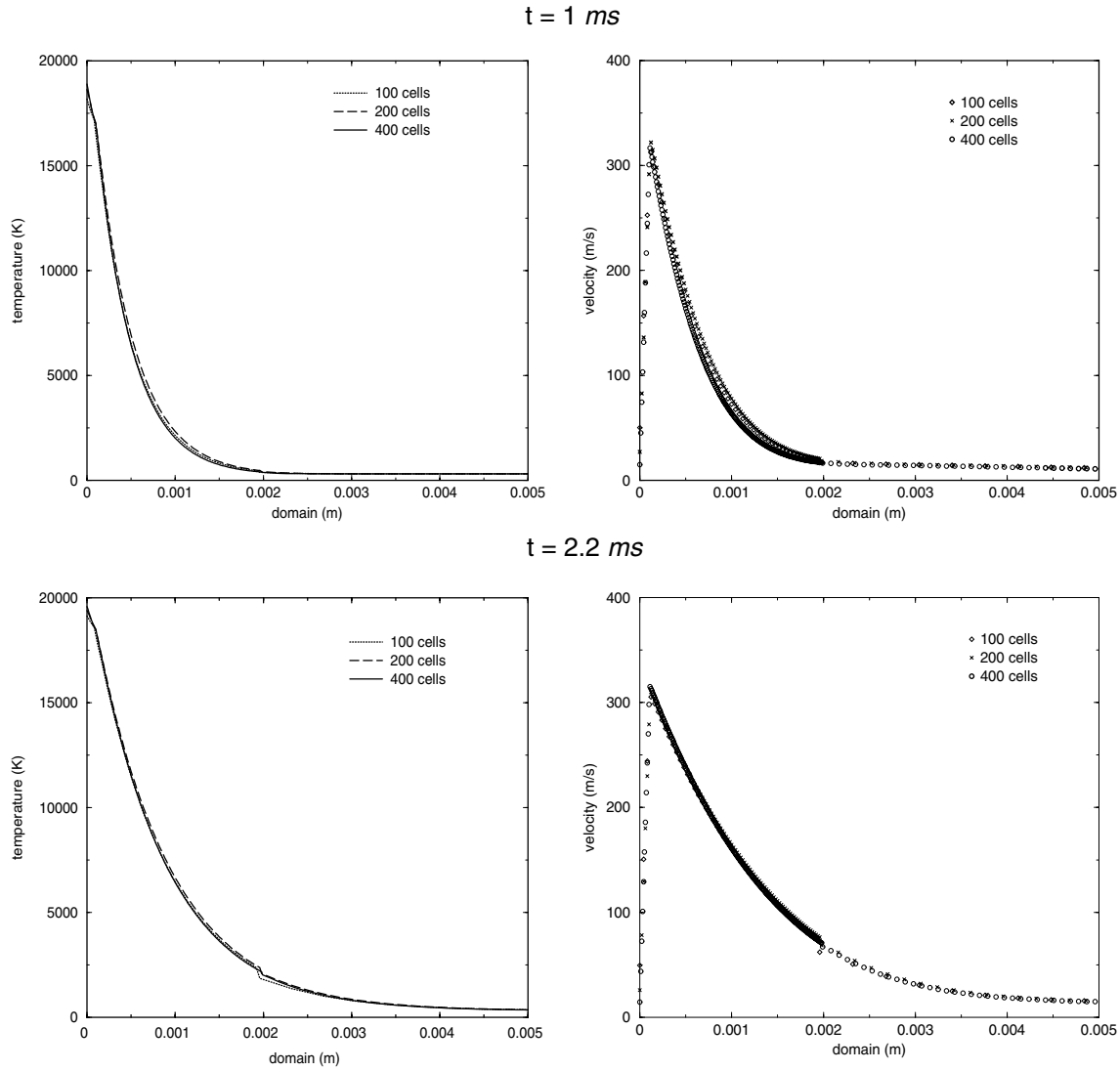

Fig. 5. Temperature and velocity distributions in the fuse domain at $t = 1$ ms representing the arc ignition and at $t = 2.2$ ms corresponding to the maximum electrical power injected in the fuse. The dotted line represents a mesh of 100 cells, dashed lines 200 cells and solid line 400 cells.

$m\,s^{-1}$ and $P_{in} = 50 \times 10^5$ Pa and we obtain $\rho_{out} = 44.3$ $kg\,m^{-3}$, $u_{out} = 4.4$ $m\,s^{-1}$ and $P_{out} = 38.2 \times 10^5$ Pa for $L = 0.1$ m. The parameters γ, ϕ, k and β are shown in Table 1 and we take $h_{sf}A_0 = 10^7$ and $T_s = 300$ K.

The numerical solution of the non-stationary problem is computed with 500 cells using the same boundary conditions $C_{in} = (\rho_{in}, u_{in}, P_{in})$ and $C_{out} = (\rho_{out}, u_{out}, P_{out})$ given by the stationary model. We assume all the gas at rest and the pressure equal to the atmospheric pressure at $t = 0$.

Fig. 4 shows the stationary solution obtained with Eq. (16) and the non-stationary solution for $t = 1$ ms and $t = 40$ ms. At $t = 1$ ms, the gas flow in porous medium is not yet stationary, but after $t = 40$ ms, the stationary system is accomplished and the solution is equal to the semi-analytic solution.

6. Numerical results and discussion

We present a simulation of an electrical arc discharge through the porous medium in a HBC fuse using realistic physical parameters. We evaluate the pressure P, density ρ_g, temperature T_g and the velocity u of the gas during the fuse operation. The fuse operation is initiated when a high current produces the heating of the fuse element followed by the fusion and the vaporization of the material and next the creation of an electrical arc.

Our goal is to present the phenomenologic aspect of the fuse operation. Indeed, the value of the pressure and temperature measure in the literature depend greatly on the Darcy and Forchheimer parameters and the vaporization rate (Bussière, 2001).

6.1. Initial conditions and parameters

Computations have been performed using the C++ finite volume library OFELI (Touzani, 1998) on a 200 elements mesh composed of two uniform meshes where 100 cells correspond to the first area on a length 2 mm and 100 cells to the second area. The time step is about $\Delta t \approx 10^{-9}$ s to respect the CFL condition and satisfy the conditional scheme stability both for the homogeneous problem and the non-homogeneous problem.

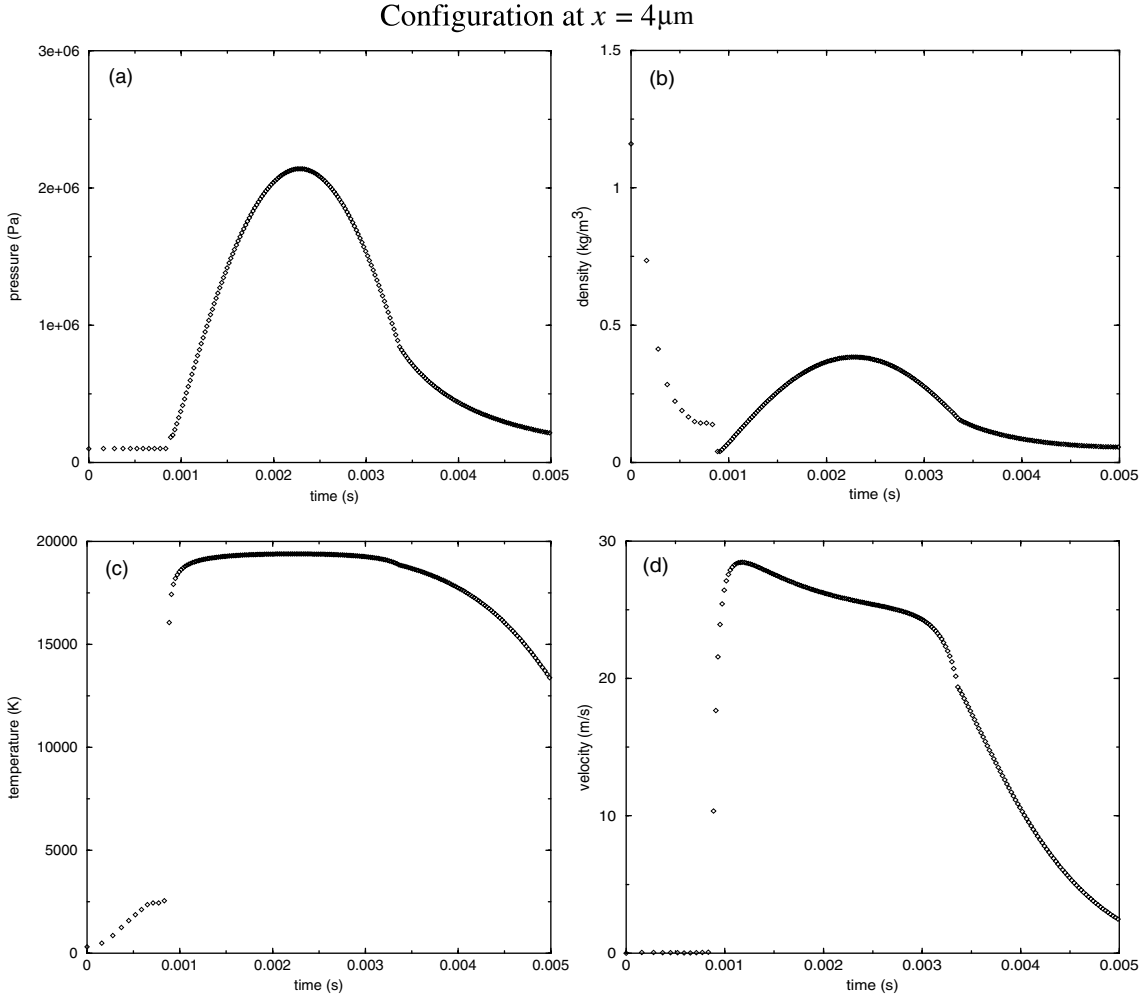

Fig. 6. Pressure, density, temperature and velocity distributions at plasma core ($x = 4$ μm) during the fuse operation ($t = 5$ ms) for a mesh of 200 cells.

At the initial time $t = 0$, the system is at rest $u = 0$ m s^{-1}, the gas present in the silica sand interstices is at atmospheric pressure and ambient temperature $T = 300$ K. The gas and silica sand parameters using in the numerical simulation are shown in Table 1.

6.2. Simulations

In order to test the precision of the numerical simulation, we consider a finest mesh composed of 50, 100, 200 uniform cells for the first area and 50, 100, 200 uniform cells for the second area. We observe a good convergence of the numerical scheme, thanks to the second order in space (MUSCL method). We note that the velocity tends to zero and the total energy $E = \rho e + 1/2\rho u^2$ is constant close to $x = 0$ to respect the symmetrical condition at $x = 0$.

During the fuse operation, we mainly observe three zones within the fuse domain determined by the gas temperature repartition (see Fig. 5). The first area is characterized by the plasma core where the gas temperature is greater than 15 000 K corresponding to the temperature where the ionized species are majority. The second area corresponds to the temperature included between 15 000 and 5000 K representing the plasma periphery and the last area is located far from the plasma where the gas temperature is lower than 5000 K. During the process, the core and periphery plasma areas expand and the numerical simulation shows that at $t = 1$ ms the plasma length is about 0.7 mm and at $t = 2.2$ ms is about 1.3 mm. The fulgurite creation which is a complex combination of molten and vaporized fuse-element metal and silica sand takes place in the area between 2 and 4 mm where the temperature is of the same order than the vaporization temperature. In the experimental tests (Jakubiuk and Lipski, 1993), authors show that the fulgurite is situated in a area about 1 cm of the plasma core, i.e. a little farer than in our simulation.

Figs. 6–8 show the pressure, density, velocity and temperature evolution during the fuse operation in the three characteristic areas of the fuse domain: plasma core ($x = 4$ μm), plasma periphery ($x = 1$ mm) and silica sand solid ($x = 15$ mm). The simulation is based on the electrical power injected in the fuse used in an experimental framework (Bussière and Bezborodko, 1999), it

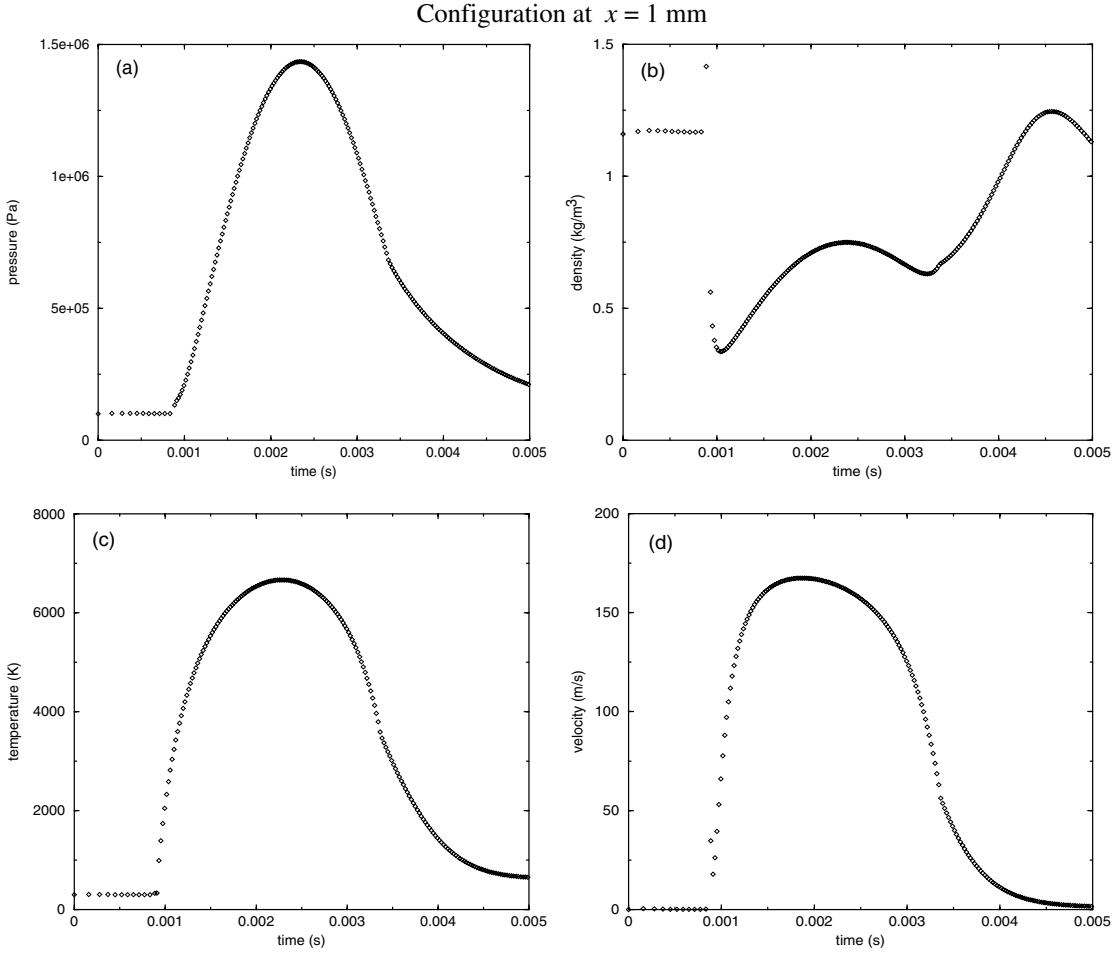

Fig. 7. Pressure, density, temperature and velocity distributions at plasma periphery ($x = 1$ mm) during the fuse operation ($t = 5$ ms) for a mesh of 200 cells.

can be decomposed in four steps: the pre-arcing period (0–0.8 ms), the arcing period where the injected power reaches the maximum power (0.8–2.2 ms), the drop of electrical power (2.2–4 ms) and the post-discharge period (4–5 ms) where the injected power vanishes.

During the pre-arcing period, the silver fuse element is overheated leading to a low vaporization of the surrounding material and the gas temperature reaches the vaporization temperature (Fig. 6(c)) leading to gas ejection toward the silica sand and a density drop ($\rho \approx 0$) (Fig. 6(b)).

When the arc is initiated ($t = 0.8$ ms), the injected power in the fuse element increases rapidly inducing a higher vaporization of material and increasing the pressure about 2 MPa in the core plasma (Fig. 6(a)) with low gas velocity (Fig. 6(d)). Note that the pressure maximum in core (Fig. 6(a)) and periphery (Fig. 7(a)) plasma coincides to the maximum of the electrical power injected (Fig. 3). Moreover the precision of the numerical scheme is satisfying, the temperature and the velocity for the two meshes are similar. We note a difference of 3×10^5 Pa for the pressure maximum due to the small variation of the density.

At the periphery plasma, the pressure is also important (Fig. 7(a)) but the temperature is reduced by a factor of 3 to reach 6000 K (Fig. 7(c)). The pressure gradient induces subsonic gas velocity in the plasma periphery (Fig. 7(d)).

Far from the arc column plasma, the temperature is constant around $T_g = 300$ K, the gas energy has been absorbed by the silica sand in the first centimeter (Fig. 8(c)).

When the power injected decreases $t \in [2.5, 5]$ ms, the arc pressure drops due to the lower vaporization of the material and the arc energy is absorbed by the silica sand (Fig. 6(c)) in the plasma core. At the plasma periphery, the temperature decreases quickly, so the periphery area is a propitious zone for the fulgurite deposition.

During the post-discharge period, i.e. when the electrical arc do not supplied, the pressure drops to the atmospheric pressure in all the fuse. Thus, there is no mechanical interaction between the gas and the silica sand in the fuse. On the other hand, the high temperature in the plasma core is maintained since the thermal conductivity between the grains of silica sand is small.

In order to evaluate the mechanical effects in the fuse, we present in Fig. 9 the repartition of the Darcy and

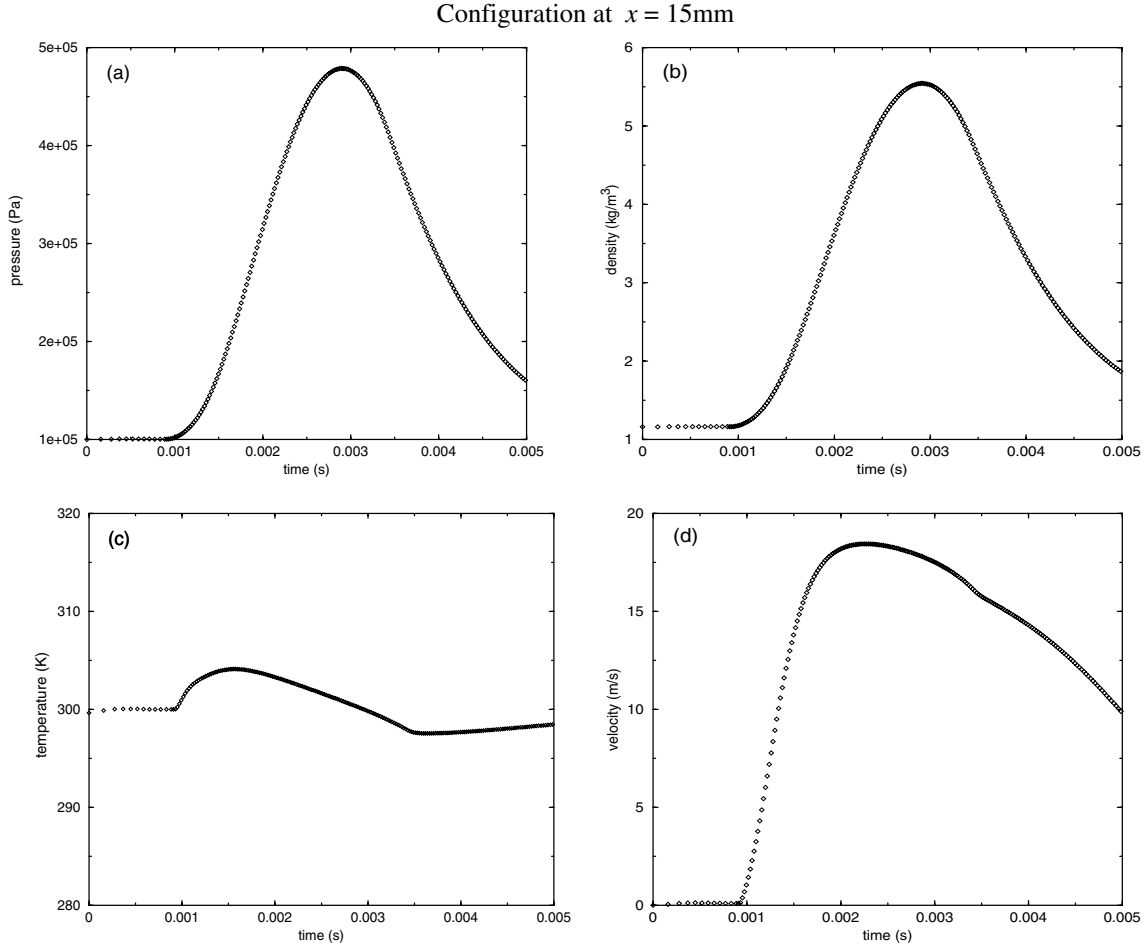

Fig. 8. Pressure, density, temperature and velocity distributions at the position $x = 15$ mm during the fuse operation ($t = 5$ ms) for a mesh of 200 cells.

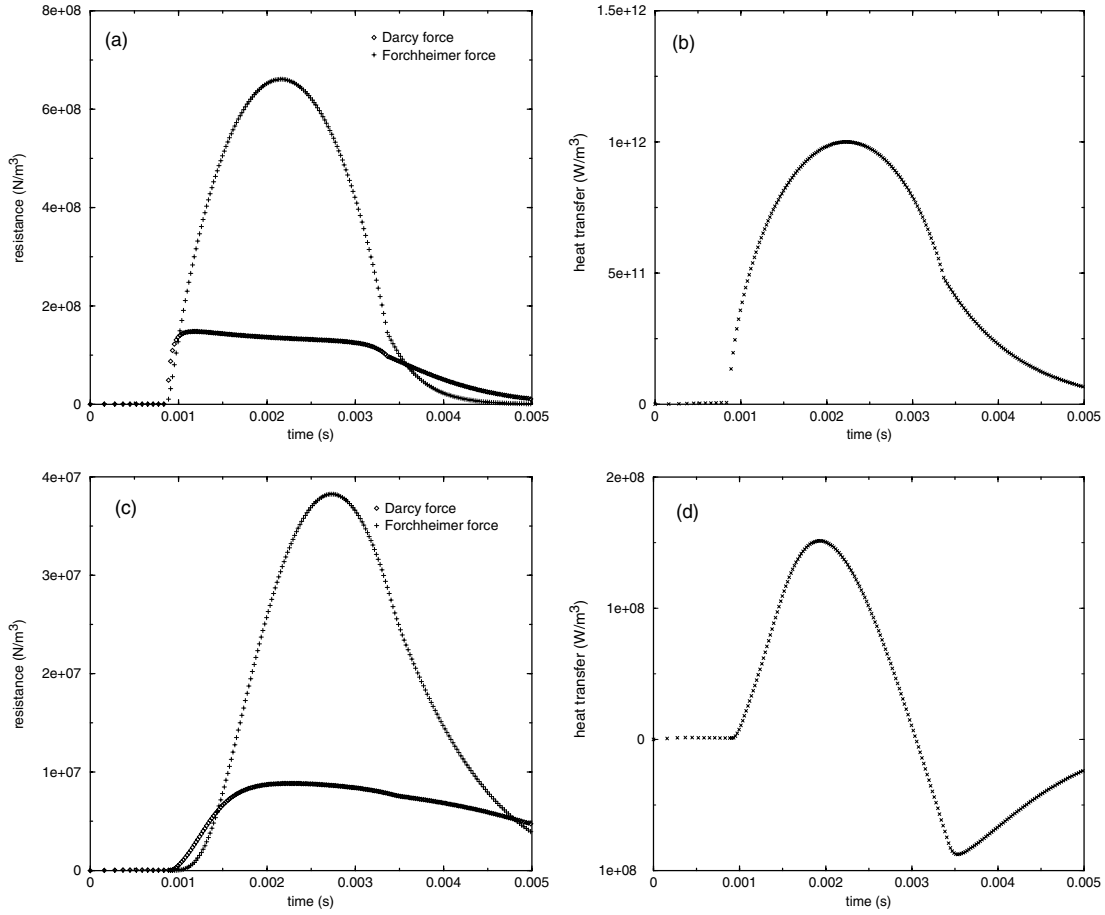

Fig. 9. The Darcy ($\diamondsuit$), Forchheimer ($+$) forces and heat transfer ($\times$) are shown for the positions $x = 100$ μm (a), (b) and $x = 15$ mm (c), (d) during the fuse operation.

Forchheimer forces and the heat transfer with respect to the time at different positions of the fuse domain: plasma periphery ($x = 100$ μm) and silica sand solid ($x = 15$ mm).

The Forchheimer force mainly governs the gas evolution on the periphery (Fig. 9(a)) and allows to keep up a high pressure around the arc column. Far from the plasma, the Forchheimer force is also preponderant (Fig. 9(c)) but outflow boundary conditions make the gas velocity higher than in reality, thus the Forchheimer force is certainly over estimated in comparison with the Darcy force far from the plasma.

The heat transfer takes place in the first millimeters which are characterized by few grains of silica sand (Fig. 9(b)), far from the plasma, the heat transfer is negligible in comparison with the plasma periphery (Fig. 9(d)). Likewise, outflow boundary condition leads to the interfacial heat transfer coefficient and the Reynolds number to be over estimated.

In the fuse operation, the vaporized mass contribution is a major fact since it contributes to increase the pressure in the arc column favouring the circuit energy dissipation and thus the interruption of the short-circuit current. Fig. 10 shows the total mass produced resulting of the material vaporization during the arcing period. The total mass is given by

$$\text{total mass} = S \int_0^{t_f} \int_0^L r(x,t)\,\mathrm{d}x\,\mathrm{d}t, \tag{17}$$

where $S = L_y.L_z = 3.5 \times 10^{-4}$ m^2 is a characteristic surface of the plasma area, t_f is the final time.

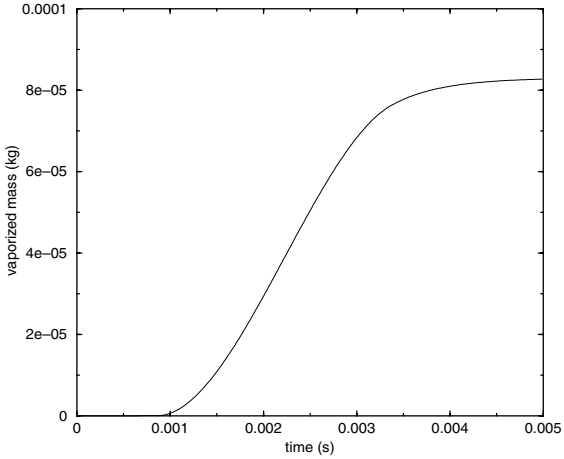

Fig. 10. Total vaporized mass during fuse operation.

The vaporized mass is produced at the beginning of the arcing period (0.9 ms) when the arc is initiated and increases as long as the injected power no vanishes. Numerical simulation gives that the total mass vaporized is approximately 0.08 g. A few quantity of material injected into the fuse leads to a high pressure in the plasma in accordance with Bussière and André (2001).

7. Conclusions

A non-stationary model for the simulation of the gas release through a porous medium with thermal non-equilibrium in a HBC fuse was developed. The model has been implemented using a finite volume solver with a fractional step technique for a one-dimensional geometry. The numerical simulation with realistic physical parameters for the silica sand used in industrial fuses gives a description of the pressure, the temperature, and the gas velocity evolution in the plasma core and the plasma periphery in adequacy with experimental measurements (Jakubiuk and Lipski, 1993). We have observed that the high plasma pressure 2 MPa is maintained due to the conjunction of a high temperature, the gas produced by vaporization and the Forchheimer force. This model gives satisfying estimates of the physical parameters in the plasma core and the plasma periphery but far from the plasma, the outflow boundary condition induces gas velocity too large. Moreover, the created vapours must be recondensed to avoid a material heap in the fuse.

Future works will consist in realizing a more complete model with species differentiation (Ag, SiO_2, air) allowing to condense the material and to predict the silver vapor motion in the silica sand.

Acknowledgements

Both authors would like to thank M.R. Barrault of Schneider Electric, R. Dides and S. Melquiond of Alstom, M.R. Rambaud of Ferraz S.A. and J.C. Vérité of Electricité de France for their financial support and for their motivating discussions. We also thank T. Buffard for many discussions in the field of the numerical simulations and R. Touzani for the advice on library OFELI.

References

Abgrall, R., 1988. Generalisation of the Roe scheme for the computation of mixture of perfect gases. Rech. Aérospatiale 6, 31–43.

André, P., Brunet, L., Duffour, E., Lombard, J.M., 2002. Composition and thermodynamic properties calculated in plasma formed insulator vapours of PC and POM at fixed volume. Eur. Phys. J.: Appl. Phys. 17, 53–64.

Bortolozzi, R.A., Deiber, J.A., 2001. Comparison between two- and one-field models for natural convection in porous media. Chem. Eng. Sci. 56, 157–172.

Bussière, W., 2000. Mesure des grandeurs (T, N_e, P) au sein du plasma d'arc des fusibles en moyenne tension. Ph.D. Thesis, Blaise Pascal University (in French).

Bussière, W., 2001. Influence of sand granulometry on electrical characteristics, temperature and electron density during high voltage fuse arc extinction. J. Phys. D 34, 925–935.

Bussière, W., André, P., 2001. Evaluation of the composition, the pressure, the thermodynamic properties and the monoatomic spectral lines at fixed volume for a SiO_2–Ag plasma in the temperature range 5000–25 000 K. J. Phys. D 34, 1657–1664.

Bussière, W., Bezborodko, P., 1999. Measurements of time-resolved spectra of fuse arcs using a new experimental arrangement. J. Phys. D 32, 1693–1701.

Claessens, M., Möller, K., Thiel, H.G., 1997. A computational fluid dynamics simulation of high- and low-current arcs in self-blast circuit breakers. J. Phys. D, 1899–1907.

Courant, R., Friedrichs, K.O., 1948. Supersonic Flow and Shock Waves. Interscience Publishers, New York.

De Ville, A., 1996. On the properties of compressible gas flow in a porous media. Transport Porous Med. 22, 287–306.

Jakubiuk, K., Lipski, T., 1993. Dynamics of fulgurite formation during arcing in HRC fuses. J. Phys. D 26, 424–430.

Jiang, P.X., Ren, Z.P., 2001. Numerical investigation of forced convection heat transfer in porous media using a thermal non-equilibrium model. Int. J. Heat Fluid Flow 22, 102–110.

Lakshiminarashima, C.S., Barrault, M.R., Oliver, R., 1978. Factors influencing the formation and structure of fuse fulgurite. IEE Proc.: Sci. Meas. Technol. 125, 391–399.

Macdonald, I.F., El-Sayed, M.S., Mow, K., Dullien, F.A.L., 1979. Flow through porous media—the Ergun equation revisited. Ind. Eng. Fundam. 18 (3).

Nielsen, T., Kaddani, A., Zahrai, S., 2001. Modelling evaporating metal droplets in ablation controlled electric arcs. J. Phys. D 34, 2022–2031.

Rochette, D., Clain, S., 2003. Numerical simulation of Darcy and Forchheimer force distribution in a HBC fuse. Transport Porous Med. 53, 25–37.

Rohsenow, W.M., Hartnett, J.P., Cho, Y.I., 1998. Handbook of Heat Transfer. McGraw-Hill Handbooks, New York.

Teng, H., Zhao, T.S., 2000. An extension of Darcy's law to non-Stokes flow in porous media. Chem. Eng. Sci. 55, 2727–2735.

Toro, E.F., 1997. Riemann Solvers and Numerical Methods for Fluid Dynamics. Springer-Verlag, Berlin.

Touzani, R., 1998–2001. Object Finite Element Library Copyright ©1998–2001 Rachid Touzani. Available from <http://www.lma.univ-bpclermont.fr/~touzani/ofeli.html>.

Turner, H.W., Turner, C., 1973. Phenomena occurring during the extinction of arcs in fuses. In: Proc. 2nd Int. Symp. on Switching Arc Phenomena, Lodtz, Poland, September 1973, pp. 253–256.

Wakao, N., Kaguei, S., 1982. Heat and Mass Transfer in Packed Beds. Gordon and Breach Science, New York.

Whitaker, S., 1996. The Forchheimer equation: a theoretical development. Transport Porous Med. 25, 27–61.

Yee, H., 1987. Upwind and symmetric shock-capturing schemes. NASA Technical Memorandum 89464.